Chemical Engineering & Technology

Chemical & Engineering Technology

RESEARCH ARTICLE OPEN ACCESS

Dust Cake Pressure Drop Determination of Surface Filters at Low Absolute Pressures

Vanessa Löschner | Jörg Meyer | Achim Dittler

KIT, Institute of Mechanical Process Engineering and Mechanics (MVM), Research Group Gas Particle Systems, Karlsruhe, Germany

Correspondence: Vanessa Löschner (vanessa.loeschner@kit.edu)

Received: 29 January 2026 | **Revised:** 26 March 2026 | **Accepted:** 16 April 2026

Keywords: filter cake pressure drop | gas particle filtration | low absolute pressure | surface filtration

ABSTRACT

Some gas particle separation processes operate at low absolute pressure, where surface filter media are widely used. Yet filter cake pressure drop behavior at these conditions remains underexplored. To improve understanding, we determined the filter cake pressure drop as a function of absolute pressure for filter cakes formed on two different surface media at a single filter face velocity. The filter cake pressure drop decreases as absolute pressure is reduced. We adapt a semi-empirical model validated for determination of clean surface media pressure drop to filter cakes and introduce a mean empirical correction factor to reduce the experimental effort. The approach captures the trends accurately, with the simplification limited to homogeneous filter cakes.

1 | Introduction

Collection of gas borne particles plays a significant role in many industrial processes, including vacuum drying [1–5]. During the drying process, the rising vapor can entrain particles from the bulk material. To prevent contamination of downstream equipment like condensers and compressors and to enable the recovery of often expensive products, separation of these particles is necessary [6–8]. Surface filters are typically used for this purpose, as they allow for simple particle recovery and regeneration via pulse jet cleaning.

Due to the limited knowledge currently available regarding the filtration behavior of surface filters at low absolute pressures, filter systems are often designed based on findings obtained under ambient absolute pressure conditions. This frequently results in over dimensioned and therefore unnecessarily expensive filter systems. Underdimensioned filter systems, on the other hand, can negatively affect filtration performance and should thus be avoided.

One of the key differences between ambient and low absolute pressure conditions is the flow regime, typically characterized by the Knudsen number (Kn-number), defined as [9, 10]:

$$\mathrm{Kn} = \frac{\lambda}{a}. \tag{1}$$

The Kn-number expresses the ratio between the mean free path of gas molecules λ and a characteristic length scale a.

In dust cake filtration, we assume as characteristic length the mean pore diameter d_{pore} of the respective porous filter medium (FM) or filter cake (FC),

$$a = d_{\mathrm{pore}} \quad \Rightarrow \quad \mathrm{Kn} = \frac{\lambda}{d_{\mathrm{pore}}}.$$

Abbreviations: EAN, Electro-aerosol neutralizer; FCE, Faraday cup electrometer; IN, Inlet nozzle; LSM, Laser scanning microscopy; M, Measurement; MFM, Mass flow meter; PPS, Polyphenylene sulfide; RBG, Rotating brush generator; SEM, Scanning electron microscopy; SG, Sintered granular medium; SMF, Sintered metal fiber medium.

Based on the Kn-number, the following flow regimes can be distinguished [11, 12]:

- Continuum flow $0 < \mathrm{Kn} \leq 0.001$
- Slip flow $0.001 < \mathrm{Kn} \leq 0.25$
- Transition flow $0.25 < \mathrm{Kn} \leq 10$
- Molecular flow $10 < \mathrm{Kn}$

With increasing Knudsen number, the classical no-slip boundary condition no longer applies and gas molecules begin to slip along surfaces. As the Kn-number increases further, gas rarefaction becomes more pronounced, resulting in flow behavior that deviates substantially from the continuum regime.

In surface filtration, a filter cake is deposited on the filter medium whose structure differs from that of the underlying substrate. Consequently, the filter medium and the filter cake can be treated as series elements that can be characterized separately for Knudsen-number evaluation and pressure drop determination. The total pressure drop equals the sum of the pressure drop across the filter medium and the dust cake.

Several studies have investigated the filtration behavior of clean depth filters under low absolute pressure conditions [13–16]. However, due to the fundamentally different structure of surface and depth filter media, these results are not directly transferable. For clean, highly porous, fibrous, and homogeneous filter media (typical for depth filter media), a number of analytical models exist to calculate the pressure drop across different flow regimes [17–22]. These models, however, rely on structural assumptions (highly porous, fibrous, and homogeneous) that are generally not fulfilled by surface filter media.

To address the structural deviations between surface and depth filter media, we adapted a calculation model developed by Karniadakis et al., originally formulated to predict pressure drops in pipes over the entire Knudsen-number range [23, 24] and applied it for the determination of pressure drop of clean surface filter media with a wide range of structural parameters under low absolute pressure conditions. The model is based on a pressure driven Hagen–Poiseuille flow in the continuum regime, corrected by slip and rarefaction relevant at low absolute pressures (i.e., high Kn). The rarefaction correction is expressed through an empirical correction factor, α_{FM} (see Section 2.5 for details of the calculation model).

In Ref. [25], α_{FM} exhibited an approximately linear dependence on absolute pressure, implying that two measurements suffice to determine this empirical correction factor. We evaluated two practical fitting strategies for determining α_{FM}:

- two-point linear fit using pressure drop data at $p_{\mathrm{abs}} = 1000\,\mathrm{hPa}$ and 10 hPa;
- one-point fit with fixed y-axis intercept and pressure drop data at $p_{\mathrm{abs}} = 1000\,\mathrm{hPa}$, using a prescribed y-axis intercept given by the average of all tested filter media, motivated by the narrow spread of intercepts observed across $\alpha_{\mathrm{FM}}(p_{\mathrm{abs}})$ profiles.

A comparison between the measured filter medium pressure drop and those calculated using both α_{FM} determination methods showed good agreement, with the two point method yielding slightly better accuracy [25].

In preceding work, two dust cake build-up procedures were compared to assess whether the absolute pressure during cake formation affects the ensuing flow behavior and consequently, the cake structure [26]. It was shown that, down to about 25 hPa, it does not matter whether the filter cake is first formed at approximately $p_{\mathrm{abs}} \approx 900\,\mathrm{hPa}$, and the absolute pressure is subsequently reduced for flow resistance measurements, or whether the filter cake is formed directly at reduced absolute pressure where the subsequent pressure drop measurement is performed. In practice, filter cake formation is substantially faster at higher absolute pressure, because reduced absolute pressure leads to gas expansion and a lower particle number concentration, producing a dilution effect that slows dust cake growth, provided the aerosol generator is operated at a constant setpoint. The filter cake build-up methodology is detailed in Section 2.4.

In the present work, we systematically investigate the pressure-drop behavior of filter cakes under reduced absolute pressure. Filter cakes are formed on two different surface filter media, a sintered metal fiber medium (SMF) and a coated sintered granular medium (SG). The sintered metal fiber medium exhibits a homogeneous surface, which strongly promotes uniform filter cake build-up, making it particularly suitable for investigations of filter cake pressure drop. By contrast, the sintered granular medium inherently exhibits more heterogeneous surface characteristics. The total pressure drop is recorded at absolute pressures of $p_{\mathrm{abs}} = 900, 500, 250, 100, 50, 25, 10,$ and 5 hPa at a constant filter face velocity of $v_F = 5.5\,\mathrm{cm\,s^{-1}}$. This filter face velocity lies at the upper end of industrial practice and enables rapid filter cake formation.

To place these measurements in a predictive context, we build on our previous work, in which the model of Karniadakis et al. was adapted and validated for calculating the pressure drop of clean surface media at reduced absolute pressure, and we now assess its applicability to filter cakes. To represent filter-cake-specific morphology and rarefaction effects, we introduce an empirical correction factor α_{FC}, identified from pressure drop measurements over a wide absolute pressure range. Model performance is validated by back calculating filter cake pressure drop from α_{FC} and comparing it with experimental data.

In addition, a filter-medium-specific mean $\bar{\alpha}_{\mathrm{FC}}$ was determined from three independently built filter cakes, together with mean structural filter cake parameters (mean porosity $\varepsilon_{\mathrm{FC,mean}}$ and mean pore diameter $d_{\mathrm{pore,FC,mean}}$). Then these mean parameter were used to back calculate filter cake pressure drop. If the deviations between the calculated and measured filter cake pressure drop remain within an acceptable range, $\bar{\alpha}_{\mathrm{FC}}$ can be, for example, reused in subsequent work to determine filter cake pressure drop at reduced absolute pressures without repeating low absolute pressure measurements and additional filter cake structure characterizations. Importantly, α_{FC} is filter medium dependent, particularly at small filter cake thicknesses. Therefore, a separate $\bar{\alpha}_{\mathrm{FC}}$ is required for each filter medium.

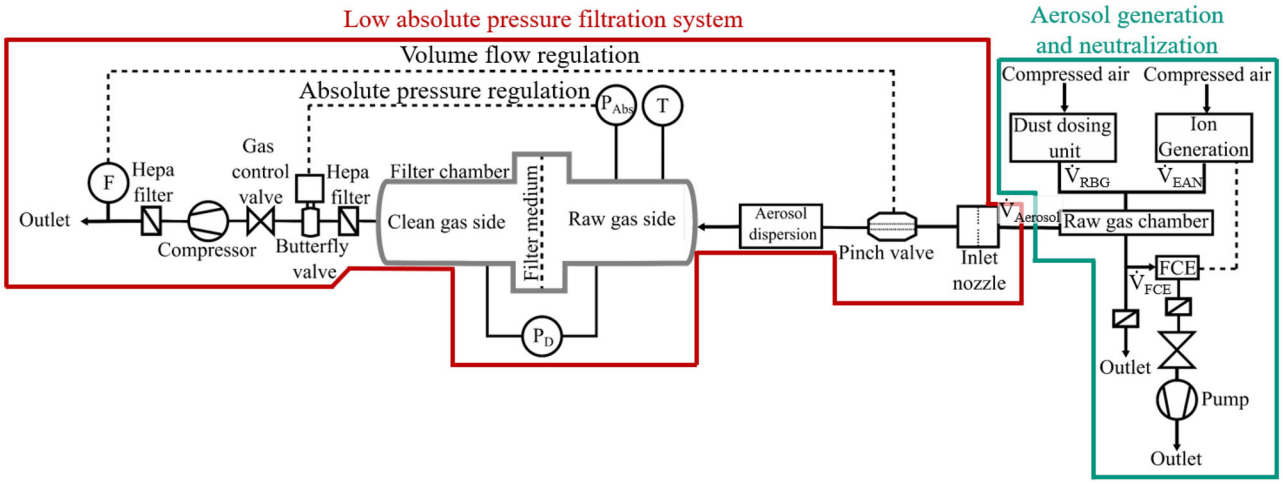

FIGURE 1 | Schematic overview of the experimental set-up. Labeled in red: filtration system (at low absolute pressure), labeled in green: aerosol generation and neutralization (at ambient conditions).

2 | Materials and Methods

2.1 | Experimental Set-Up

In this study, a test rig specifically designed for low absolute pressure surface filtration conditions is used. A schematic illustration of the experimental setup is shown in Figure 1. The setup can be divided into two main components: the low absolute pressure filtration system and the aerosol generation and neutralization unit, which are described in the following sections. A brief overview of the setup is provided here. A more detailed description can be found in [26].

2.1.1 | Aerosol Generation and Neutralization

The aerosol generation and neutralization set-up is outlined in green in Figure 1. The aerosol is generated using an RBG 1000 aerosol generator (Palas GmbH), operated at a constant pre-pressure of 1.4 bar, producing a stable volumetric flow rate of 53 L min^{-1}. Since the aerosol generated by the dust dosing unit typically carries a substantial electrostatic charge, it must be neutralized to minimize particle losses and avoid effects caused by particle charging.

Neutralization is achieved using ions generated by the EAN 581 (Topas GmbH) via corona discharge. The resulting charge state of the aerosol is monitored with a Faraday Cup Electrometer (FCE) to verify effective neutralization. Neutralization is verified by a reduction of at least one order of magnitude in total aerosol charge; detailed data are reported in Ref. [26]. The volumetric flow rate provided by the EAN 581 is 45 L min^{-1}, resulting in a total volumetric flow rate into the raw gas chamber of 98 L min^{-1}. The raw gas chamber is integrated into the setup to increase aerosol residence time and ensure a more stable aerosol concentration.

Depending on the absolute pressure on the raw gas side and the filter face velocity, a specific volumetric flow rate is drawn into the filter chamber. The volumetric flow not drawn into the filter chamber is routed via a bypass through filters and then discharged to the environment.

2.1.2 | Low Absolute Pressure Filtration System

The aerosol volumetric flow rate drawn into the filter chamber is first coarsely adjusted using inlet nozzles (IN). A nozzle with a diameter of $d_{IN,1} = 2.94$ mm is used for larger flow rates (up to 46 L min^{-1}), while a smaller nozzle with $d_{IN,2} = 1.36$ mm is used for low flow rates (below 10 L min^{-1}).

Fine adjustment of the volumetric flow rate is performed using a pneumatically actuated pinch valve. The aerosol then passes through an aerosol dispersion unit, which divides the stream into four pipes, evenly distributed across the inlet section, assuming a uniform aerosol distribution across the raw gas cross section of the filter chamber.

On the raw gas side of the filter chamber, the temperature (Pt 100, 4-wire) and the absolute pressure (vacuum transmitter Pirani from Thyracont Vacuum Instruments GmbH) are measured. The transmitter covers 5×10^{-5} mbar to 2000 mbar with stated precision of <2% for 2000–200 mbar, <5% for 200–40 mbar and <10% for 40–2×10^{-3} mbar. The pressure drop across the filter medium is monitored using differential pressure transmitters from ICS Schneider Messtechnik GmbH with measuring ranges up to 50 and 200 mbar, respectively. Downstream of the filter chamber, two valves (a butterfly valve [VAT Group AG] and a gas control valve [EVR 116, Pfeiffer Vacuum GmbH]) are used to adjust and maintain the absolute pressure on the raw gas side of the filter chamber. To establish the flow through the experimental setup, a Pfeiffer Vacuum DUO 120 M compressor is used. The resulting volumetric flow rate through the filter chamber is measured downstream using two thermal mass flow meters (MFM, MKS Instruments Deutschland GmbH), selected according to the flow rate to be measured and placed after the compressor. The MFMs have full scale ranges of 50 and 2 L min^{-1}, respectively.

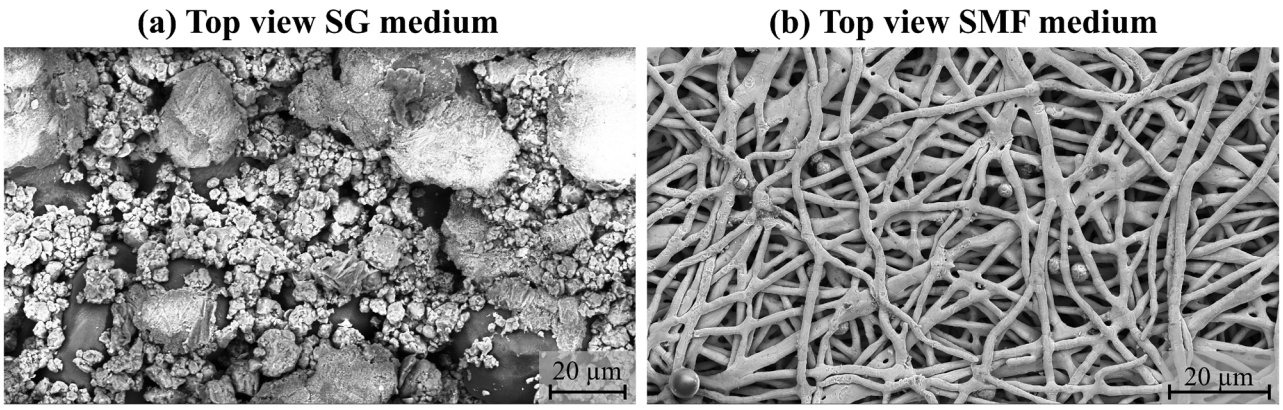

FIGURE 2 | SEM image of the upstream surface of the (a) SG medium (b) SMF medium.

TABLE 1 | Key structural parameters of the filter media.

Filter medium	Thickness L_{FM} / mm	Basis weight W_{FM} / g m^{-2}	Mean porosity $\varepsilon_{FM\,mean}$ / –	Mean filter medium pore diameter $d_{pore,FM\,mean}$ / µm
SMF	0.45[a]	1200[a]	0.67[a]	1.36[a]
SG	4[d], [a]	2148[a]	0.46[c]	4.82[b]

[a]Data from datasheet.
[b]Determined by capillary porometry.
[c]Computed as $\varepsilon = 1 - \frac{W_{FM}}{\rho_{FM} L_{FM}}$, where ρ_{FM} is the filter medium density.
[d]Total thickness of the SG (support plus surface coating).

2.2 | Filter Media

Two surface filter media were investigated: a non-woven sintered metal fiber medium (hereafter "SMF") and a rigid surface filter medium produced by sintering polyethylene (PE) granulate (hereafter "SG"). Scanning electron microscope (SEM) images of both media are shown in Figure 2.

The SG medium features an additional thin surface coating of sintered polyphenylene sulfide (PPS) granulate. This coating is not fully homogeneous. Due to the two-layer structure, the PPS layer largely controls the mean pore size, whereas the supporting structure exhibits substantially larger pores. Appendix A quantifies this structural inhomogeneity by porometry-based cumulative pore size distributions $Q_0(d_{pore})$ of the SG medium with and without PPS coating. The coating shifts the pore structure toward smaller pore diameters, with d_{50} decreasing from 28.64 to 4.82 µm, while the large span $((d_{90} - d_{10})/d_{50})$ of 6.29 indicates that a noticeable fraction of larger pores still remains.

The SMF medium consists of nonwoven fibers with an average diameter of approximately 1 µm. The fibers are made of AISI 316L stainless steel (CrNiMo steel) and are consolidated by sintering. Owing to the dense fiber packing, the medium exhibits a highly uniform and structurally homogeneous surface.

The key structural parameters of both filter media are summarized in Table 1. For dust cake formation, either a new medium or a previously cleaned medium was used. The cleaning procedure is described in [26].

2.3 | Test Dust

The test dust used in this study is Mikhart MU08 from Provencale S.A., a ground calcium carbonate $CaCO_3$. It is a white, fine powder with a strong tendency to agglomerate.

Mikhart MU08 exhibits a volume based median particle diameter ($d_{50,3}$) of approximately 1 µm and a relative span ($\frac{d_{90,3} - d_{10,3}}{d_{50,3}}$) of 2.03, as determined offline by laser diffraction. This particle size range corresponds to particles that can be entrained by ascending vapor during vacuum drying and thus must be effectively separated by the filtration system.

2.4 | Dust Cake Build-Up

The method for dust cake build-up used in this work is shown in Figure 3. To determine the pressure drop across the dust cake as a function of absolute pressure, dust cakes were generated at an absolute pressure of 900 hPa. After a filter loading time of approximately 2.5 h, the aerosol generation was stopped. Subsequently, the absolute pressure was reduced stepwise down to 5 hPa, and the resulting total pressure drop was recorded at each absolute pressure stage.

After determining the filter medium pressure drop, the filter cake pressure drop for each stage can be calculated as:

$$\Delta p_{FC} = \Delta p_{Tot} - \Delta p_{FM}. \quad (2)$$

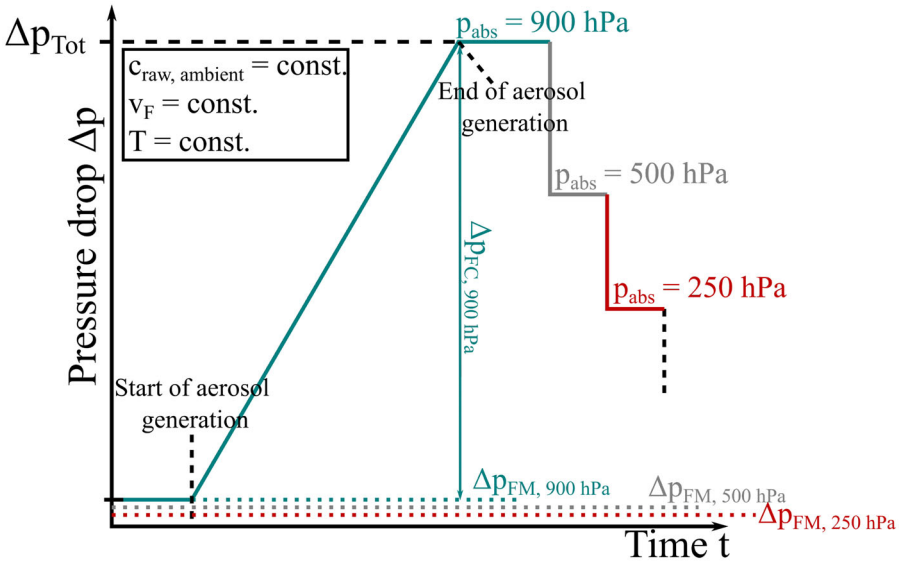

FIGURE 3 | Schematic procedure for dust cake formation at ambient conditions and subsequent stepwise absolute pressure reduction [26].

The build-up method used here does not allow determination of the filter medium pressure drop at every absolute pressure stage. For each sample, Δp_{FM} is known only at 900 hPa. However, from previous work, filter medium pressure drops for each absolute pressure stage for one representative sample are available for the SG medium [25]. For the SMF medium, the same sample was used throughout the experiments and had been pre-characterized for Δp_{FM} at all absolute pressure stages. Because filter cake pressure drops vary markedly between different SG samples, accurate filter cake pressure drop evaluation requires sample-specific Δp_{FM} data. To obtain this, the Δp_{FM} at other stages is calculated on a sample-specific basis by scaling the sample-specific Δp_{FM} value at 900 hPa with absolute pressure stage ratios taken from the representative dataset, under the assumption that these ratios are sample invariant [26]. This assumption was additionally assessed in Appendix B. The comparison between predicted and directly measured Δp_{FM} values for both filter media showed overall good agreement, with larger relative deviations only at the lowest absolute pressure stages where the absolute Δp_{FM} values are very small.

During the initial phase of dust deposition, both filter media exhibit a nonlinear increase in total pressure drop before the subsequent approximately linear cake build-up regime is reached, as illustrated by the representative $\Delta p(t)$ curves shown in Figure C.1. This effect is more pronounced for the SG medium. Possible reasons for this initially steep increase in total pressure drop include preferential loading of more permeable regions, internal deposition, and briefly elevated particle concentrations immediately after switching on the aerosol supply. Accordingly, the schematic representation in Figure 3 idealizes both the onset of dust deposition and the transition to the subsequent cake build-up regime and therefore does not reproduce the detailed course of the experimental $\Delta p(t)$ curves. For the present model calculation, the full pressure drop increase during dust deposition is assigned to filter cake build-up. A more detailed discussion of the possible mechanisms, the underlying reasoning for this evaluation approach, and a conservative uncertainty estimate are given in Appendix C.

Previous studies have shown that, for each absolute pressure stage, the resulting specific filter cake constant C_{FC} is nearly identical to the value obtained when the filter cake is formed directly at that absolute pressure, indicating that the filter cake structure remains unchanged during absolute pressure reduction [26].

2.5 | Calculation Model

The structure of surface filter media and dust cakes is highly complex and cannot be represented in full detail [27]. To enable a simplified calculation of the pressure drop through the filter medium and the filter cake, these complex (e.g., fibrous or porous) structures must be significantly reduced to an idealized model. The underlying model concept is illustrated in Figure 4. Both the filter medium and the dust cake are represented as a parallel arrangement of straight cylindrical channels with a constant cross section. These channels are characterized by an average pore diameter $d_{pore,mean}$ with additional subscripts FM and FC referring to the filter medium and the filter cake, respectively. In this idealization, the porosity of each layer (filter medium and filter cake) is proportional to the number density of channels per unit area.

Because the free flow cross-sectional area is reduced by the presence of the filter medium and the dust cake, the pore velocity v_{pore} in the respective layer increases inversely with the porosity of the filter medium and the dust cake:

$$v_{pore} = \frac{v_F}{\varepsilon}, \tag{3}$$

where v_F is the filter face velocity and ε is the porosity of the respective layer (ε_{FM} or ε_{FC}). We assume that the pore averaged velocity in the model channels equals the pore velocity in the real filter medium and dust cake.

The volumetric flow through a single pore is then

$$\dot{V} = v_{pore} A_{pore} = \frac{v_F}{\varepsilon} \frac{\pi}{4} d^2_{pore,mean}, \tag{4}$$

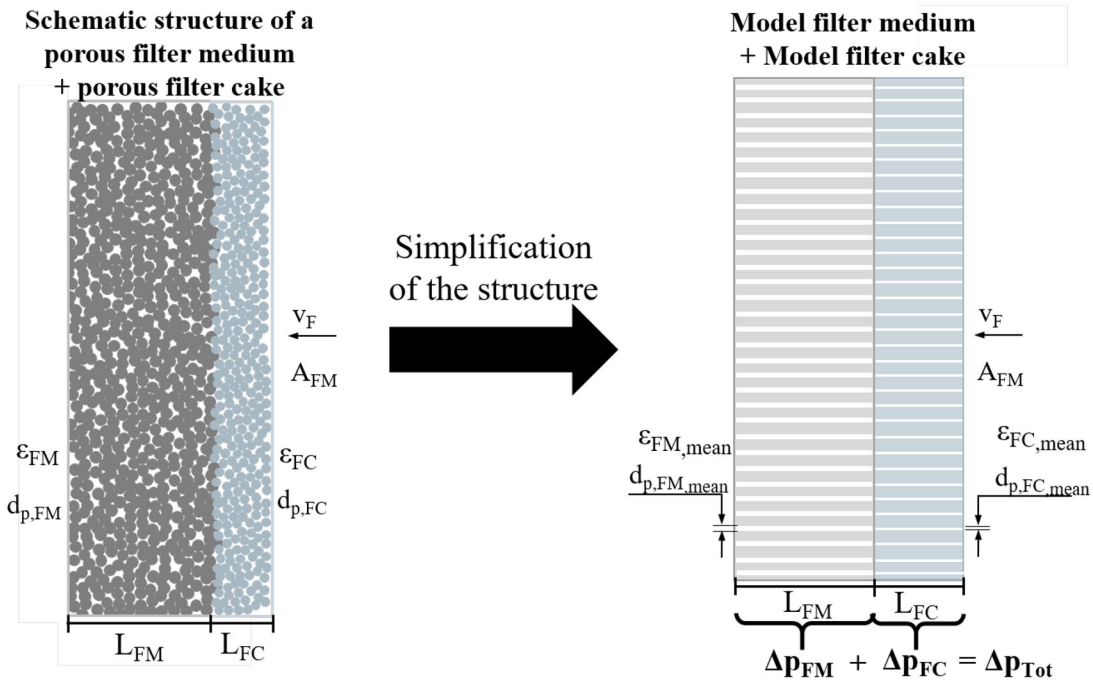

FIGURE 4 | Model structure simplification of the filter medium and the filter cake for calculating the pressure drop of surface filter media under low absolute pressure conditions.

where $A_{\text{pore}} = (\pi/4)\, d^2_{\text{pore,mean}}$ is the cross-sectional area of a pore. The single pore flow thus depends on the filter face velocity v_F, the porosity of the respective layer and the corresponding mean pore diameter.

Assuming that a micro- or nanoscale flow occurs within the idealized pores of the filter medium and filter cake, we apply the model of Karniadakis et al. (Equation 5) [23]:

$$\dot{V} = \underbrace{\frac{-\pi\left(\frac{d_{\text{pore,mean}}}{2}\right)^4}{8\mu_L}\frac{\mathrm{d}p_{\text{abs}}}{\mathrm{d}x}}_{\text{I: Hagen-Poiseuille}} \cdot \underbrace{\left(1+\frac{4\,\text{Kn}}{1-b\,\text{Kn}}\right)}_{\text{II: Slip correction}} \cdot \underbrace{(1+\alpha\,\text{Kn})}_{\text{III: Rarefaction effects}}, \tag{5}$$

with $\dot{V}$ the volumetric flow rate through a single pore, $d_{\text{pore,mean}}$ the mean pore diameter, Kn the Knudsen number, b the slip coefficient, and α an empirical correction coefficient. Equation (5) consists of three parts: Part I describes the pressure-driven Hagen–Poiseuille flow for the continuum regime, Part II corrects the volume flow due to slip effects at high Kn numbers, and Part III accounts for additional rarefaction effects that grow with Kn. A detailed discussion of each term is given in [25]. The present model does not include separate terms for pore entry/exit or cross-sectional contraction/expansion losses; these effects are subsumed in Part III together with rarefaction and are not separable from it.

In this work, we assess the applicability of the model to determine the pressure drop across dust cakes; consequently, all subsequent equations refer to filter-cake-specific quantities and use the subscript FC. The suitability of the model for clean filter media has been demonstrated elsewhere [25].

Integration of Equation (5) across the filter cake thickness L_{FC} with inlet p_i and outlet absolute pressures p_o as the boundary condition yields

$$L_{\text{FC}} = \underbrace{\frac{-\pi\left(\frac{d_{\text{pore,FC,mean}}}{2}\right)^4}{8\mu_L\,\dot{V}}}_{C_1} \times \left[\frac{4C_2 b + 4C_2\alpha\,\ln(p_o - C_2 b) + (C_2\alpha b - 4C_2\alpha)\,\ln(p_o) + b\,p_o}{b} - \frac{4C_2 b + 4C_2\alpha\ln(p_i - C_2 b) + (C_2\alpha b - 4C_2\alpha)\ln(p_i) + b\,p_i}{b}\right], \tag{6}$$

with

$$C_2 = \frac{k_B T}{\sqrt{2}\,\pi\, d^2\, d_{\text{pore,FC,mean}}},$$

where p_o and p_i are the absolute pressures downstream and upstream of the filter cake, L_{FC} is the filter cake thickness and C_2 is a fluid- and material specific constant that depends on the Boltzmann constant k_B, the temperature T, the molecular diameter d (for air, $d = 3.5 \times 10^{-10}$ m), and the mean filter cake pore diameter $d_{\text{pore,FC,mean}}$. Equation (6) further depends on the gas viscosity μ_L and the volumetric flow rate $\dot{V}$.

The pressures p_o and p_i are not measured directly. Instead, the total pressure drop Δp_{tot} across the filter medium and dust cake and the absolute upstream pressure p_{abs} are measured. The

downstream pressure (p_o) follows from

$$p_o = p_{\text{abs}} - \Delta p_{\text{tot}}.$$

Moreover, the pressure immediately upstream of the filter cake is

$$p_i = p_{\text{abs}} - \Delta p_{\text{FM}},$$

where Δp_{FM} denotes the pressure drop across the clean filter medium alone. The procedures for determining Δp_{FM} and Δp_{tot} are detailed in Section 2.4.

However, to calculate the pressure drop of filter cakes, the mean porosity and mean pore diameter are also required. For the dust cake, the mean porosity can be determined using Equation (7):

$$\varepsilon_{\text{FC,mean}} = 1 - \frac{\rho_{\text{FC}}}{\rho_P} = 1 - \frac{m_{\text{FC}}}{\rho_P A_F L_{\text{FC}}}. \tag{7}$$

Here, m_{FC} denotes the mass of the dust cake, ρ_P is the particle density, A_F the filter face area of the filter medium, and L_{FC} the thickness of the dust cake. The mass of the dust cake is determined gravimetrically after each experiment. The cake thickness is measured using a laser scanning microscope (LSM).

To calculate the mean porosity, it is assumed that the dust cake is homogeneously distributed and fully closed. Additionally, a constant particle density and no edge deformation of the dust cake are assumed. The mean pore diameter of the dust cake can be calculated using the Carman–Kozeny equation (Equation 8). This equation assumes that the particle material consists of ideal spheres, the filter cake is randomly packed and that the pores are uniformly distributed and subject to laminar flow.

$$d_{\text{pore,FC,mean}} = \sqrt{\frac{150\, v_F\, \mu_L\, L_{\text{FC}} \left(1 - \varepsilon_{\text{FC,mean}}\right)^2}{\varepsilon^3_{\text{FC,mean}}\, \Delta p_{\text{FC,900 hPa}}}}. \tag{8}$$

Here, v_F is the filter face velocity, μ_L the gas viscosity, L_{FC} the filter cake thickness, $\varepsilon_{\text{FC,mean}}$ the mean filter cake porosity, and $\Delta p_{\text{FC,900 hPa}}$ the filter cake pressure drop measured at 900 hPa.

The Carman–Kozeny equation is formally derived for continuum flow conditions. In our system, however, the dust cakes do not attain the continuum regime even at ambient pressure (see Figure 6), and slip and rarefaction effects are therefore nonnegligible. Accordingly, the pore diameter obtained from the Carman–Kozeny relation is not interpreted as a directly measured geometric pore size. Instead, the relation is used here as a pragmatic and reproducible calculation scheme to derive an effective model parameter from measurable filter cake properties, namely filter cake thickness, porosity, and the pressure drop measured at 900 hPa. This is necessary because the calculation model requires a characteristic length scale, while a direct determination of an equally suitable pore diameter for the present thin filter cakes is not available within the experimental framework used here. The resulting $d_{\text{pore,FC,mean}}$ therefore serves as a model-compatible effective length scale rather than as a direct structural measurement. This approximation is considered reasonable because the prevailing slip flow regime remains sufficiently close to continuum conditions.

Appendix D further illustrates why this choice is used in the present work. For an exemplary SMF dataset, the Carman–Kozeny-based value yields the smallest maximum deviation between calculated and measured Δp_{FC} across the investigated absolute pressure range, while larger pore diameters quickly lead to deteriorating agreement and, beyond a threshold, to the loss of a numerical solution. The Carman–Kozeny estimate is therefore used not because it is assumed to represent the exact geometric pore size, but because it provides a simple, reproducible, and numerically robust input parameter for the pressure drop model.

Overall, the present data do not allow a direct conclusion on how specific dust properties affect α_{FC}. Within the present model, α_{FC} is linked to the effective filter cake properties used in the calculation, in particular $d_{\text{pore,FC,mean}}$, L_{FC}, and, indirectly, $\varepsilon_{\text{FC,mean}}$. In addition, the applied absolute pressure range can further affect both the position and the shape of the $\alpha_{\text{FC}}(p_{\text{abs}})$ profile, since pressure level and pore diameter jointly determine the prevailing rarefaction conditions. Accordingly, possible dust effects can only be assessed indirectly through their influence on the resulting filter cake properties.

3 | Results and Discussion

3.1 | Experimental Determination of the Filter Cake Pressure Drop

The objective of this study is to investigate the influence of absolute pressure on the pressure drop across filter cakes and to assess whether an existing model for calculating clean filter medium pressure drop can also be applied to describe the pressure drop across filter cakes.

Two different filter media were used, as described in detail in Section 2.2. To determine the filter cake pressure drop, the clean filter medium was first characterized with respect to its intrinsic pressure drop. Subsequently, a dust cake was deposited on the medium and the total pressure drop (i.e., the sum of the clean filter medium and dust cake pressure drop) was measured. The procedure for dust cake build-up and the recording of total pressure drop as a function of absolute pressure is given in Section 2.4.

Figure 5 shows the total pressure drop and the clean filter medium pressure drop as a function of the absolute pressure at a constant filter face velocity of $v_F = 5.5\,\text{cm}\,\text{s}^{-1}$ for the SMF medium (a) and the SG medium (b).

For the SMF medium, the same sample was used in all repetitions and each test was repeated three times. Only small deviations between the repetition curves (both for the total pressure drop and for the clean filter medium pressure drop) can be observed.

In contrast, for the SG medium, different samples were used for the three repetitions, which explains the larger variation in the clean filter medium pressure drop. Moreover, for the clean SG medium, only the atmospheric pressure drop data points were measured directly for each sample. The remaining values at reduced absolute pressure were reconstructed based on the

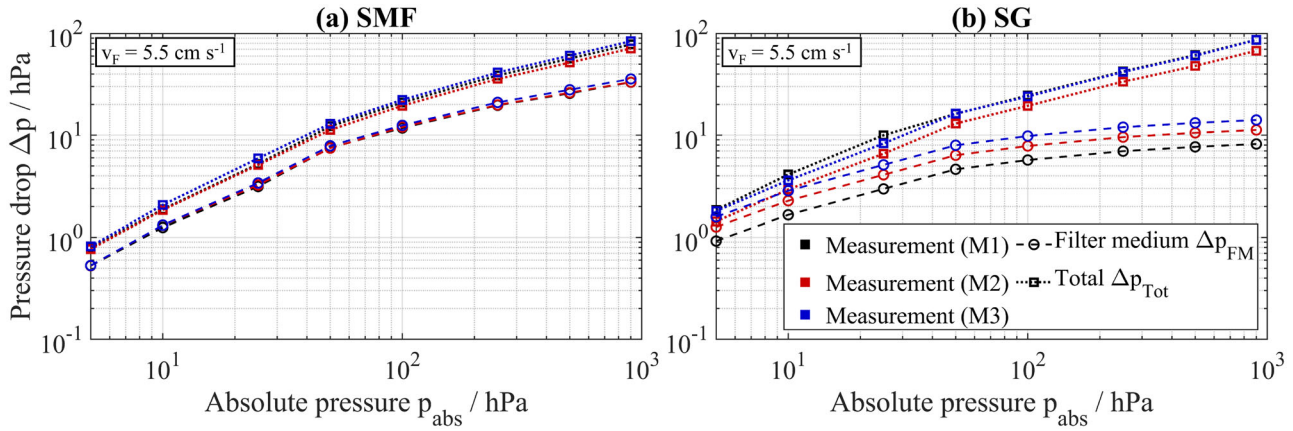

FIGURE 5 | Clean filter medium pressure drop (Δp_{FM}) and total pressure drop Δp_{Tot} ($\Delta p_{FM} + \Delta p_{FC}$) for the SMF (a) and SG medium (b) as a function of absolute pressure, measured at a constant filter face velocity of 5.5 cm s^{-1}. Three independent measurements were performed for each condition.

TABLE 2 | Key filter cake parameters for the SMF and the SG medium determined from measurements and calculations.

Medium	Measurement M	Filter cake thickness[a] L_{FC} / µm	Filter cake areal mass[b] W_{FC} / gm^{-2}	Mean filter cake porosity[c] $\varepsilon_{FC,mean}$ / –	Mean filter cake pore diameter[d] $d_{pore,FC,mean}$ / µm	Dust cake pressure drop $\Delta p_{FC,900\,hPa}$ / hPa	$\frac{\Delta p_{FC,900\,hPa}}{L_{FC}}$ / hPa µm^{-1}
SMF	1	149 ± 4	67.23	0.83 ± 0.005	0.51 ± 0.011	45 ± 0.6	0.3
SMF	2	141 ± 3	65.35	0.83 ± 0.004	0.53 ± 0.009	38.1 ± 0.6	0.27
SMF	3	211 ± 3	89.31	0.84 ± 0.002	0.52 ± 0.006	48.2 ± 1.2	0.23
SG	1	129 ± 7	57.14	0.84 ± 0.009	0.33 ± 0.014	78.5 ± 0.6	0.61
SG	2	129 ± 19	61.69	0.82 ± 0.026	0.43 ± 0.048	56.4 ± 0.6	0.44
SG	3	100 ± 21	54.54	0.79 ± 0.043	0.41 ± 0.076	72.4 ± 2.2	0.72

[a]Measured with LSM.
[b]Determined with weighed mass with $W_{FC} = \frac{m_{FC}}{A_F}$.
[c]Calculated using Equation (7).
[d]Estimated using the Carman–Kozeny equation (Equation 8).

known absolute pressure–pressure drop relationship of a separate clean filter-medium sample, as detailed in [26].

Overall, the total pressure drop decreases more strongly with decreasing absolute pressure than the clean filter medium pressure drop. This trend is consistent across repetitions and is more pronounced for the SG medium. For the SMF medium, the three total pressure drop curves agree well, whereas for the SG medium, slight deviations between repetitions are observed.

Based on Figure 5, the filter cake pressure drop can be determined using Equation (2). To isolate the filter cake contribution, the clean filter medium pressure drop is subtracted from the total pressure drop at identical operating points. For clarity, we refer to "filter cake pressure drop measurements," although the filter cake pressure drop was not measured directly but derived from filter medium pressure drop and total pressure drop measurements.

For the calculation of the filter cake pressure drop with the model introduced in Section 2.5, additional parameters are required, as already described: the filter cake mass, filter cake thickness, mean filter cake porosity, and the mean filter cake pore size. The filter cake thickness was measured using a LSM and the filter cake mass was determined by weighing. From these measurements, the mean filter cake porosity and the mean filter cake pore diameter were calculated using Equations (7) and (8), respectively. For clarity and traceability, all determined parameters for the three repetitions and both filter media are summarized in Table 2. The filter cake mass is reported as an areal mass, $W_{FC} = m_{FC}/A_F$, that is, mass per unit filtration area. Absolute deviations are reported as well for all quantities except the areal mass. The filter medium was weighed only once before and after dust loading. The balance resolution of the scales is 1 mg, while values are reported to 10 mg. Hence, balance fluctuations are expected to be at the mg level and are negligible for the present analysis. The absolute uncertainty in $\varepsilon_{FC,mean}$ originates solely from the uncertainty in L_{FC}. For $d_{pore,FC}$ the uncertainty of the pressure drop measurement was also propagated, but it is very small and has a negligible effect on the porosity uncertainty. For the filter cake thickness L_{FC}, very thin cakes (≈100 µm) can yield large relative errors (up to 21%), whereas the average relative error remains below 10%. Importantly, even these comparatively large thickness uncertainties translate into only small uncertainties in $\varepsilon_{FC,mean}$ and $d_{pore,FC,mean}$.

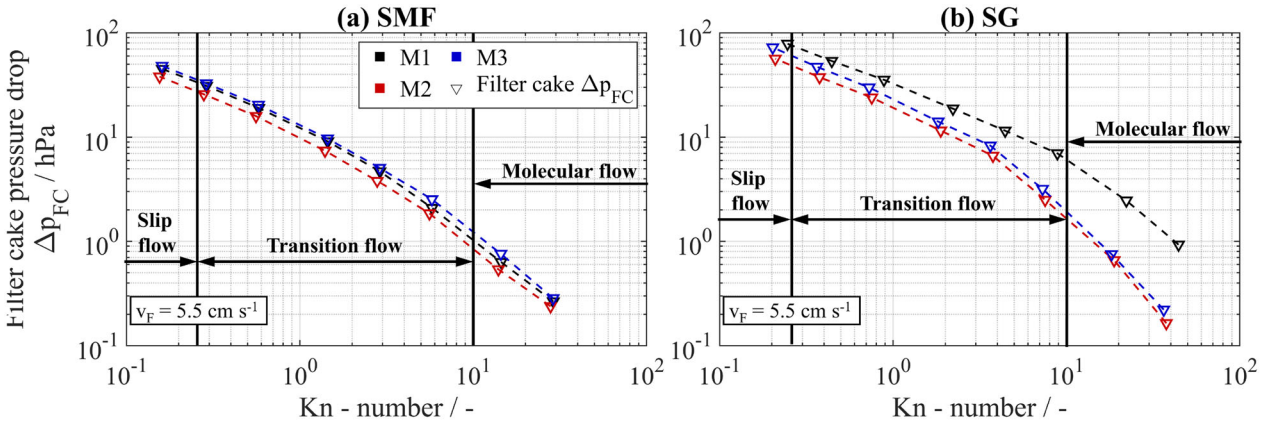

FIGURE 6 | Filter cake pressure drop for (a) the SMF medium and (b) the SG medium as a function of the Knudsen number at a constant filter face velocity of $v_F = 5.5\,\mathrm{cm\,s^{-1}}$, for all three repetitions.

Despite the comparatively high dust cake pressure drops, only thin cakes were produced (all $L_{FC} \leq 211$ µm; see Table 2). On the SMF medium, L_{FC}, W_{FC}, and Δp_{FC} exhibit an approximately linear relationship across the three repetitions. Consequently, the derived parameters $\varepsilon_{FC,mean}$ and $d_{pore,FC,mean}$ show only little scatter. The apparent homogeneity is attributable to the use of the same SMF sample for all repetitions, which minimizes the variability from substrate to substrate during dust cake formation. Consistent with this, the filter cake thickness specific filter cake pressure drop $\Delta p_{FC}/L_{FC}$ (in Pa µm^{-1}) varies only weakly across the different SMF measurements.

In contrast, the filter cakes on the SG medium do not show a clear linear dependence between L_{FC}, W_{FC}, and Δp_{FC}. Here, three different SG samples were used, and the coating of the SG medium is not homogeneous. Both factors likely contribute to the increased variability of the measured parameters. While the filter cake porosities ε_{FC} obtained on SG fall within a range similar to those on the SMF medium, the derived mean filter cake pore diameters $d_{pore,FC,mean}$ differ markedly between the two filter media.

For sufficiently thick filter cakes, one would expect the filter cake structure, and thus $d_{pore,FC,mean}$, to become less sensitive to the underlying filter medium and to converge to similar values on both filter media. However, the present dust cakes are relatively thin. Under these conditions, the developing cake structure in the near-filter-medium region can still be influenced by the filter medium structure and its induced local inhomogeneities. This does not necessarily imply that the entire filter cake is strongly inhomogeneous. Rather, the influence of the substrate is expected to be most relevant during the initial stage of deposition and for thin cakes, where the near-filter-medium region represents a substantial fraction of the overall cake thickness. The classical Carman–Kozeny approach does not account for such filter medium effects or for spatial inhomogeneity in thin cakes. Accordingly, the $d_{pore,FC,mean}$ values derived here should be interpreted with caution for very thin cakes, especially on the SG medium, where sample to sample variability and the nonhomogeneous coating are more pronounced.

Overall, the SMF filter medium yields reproducible, homogeneous filter cakes with consistent properties, whereas for the SG filter medium, a larger variability is observed. This variability likely originates from both material heterogeneity and the influence of the substrate on the developing cake structure in the near-filter-medium region, which is particularly relevant for the very thin cakes investigated here.

The filter cake pressure drop determined from the total pressure measurements as a function of the Knudsen number is shown in Figure 6 for a constant filter face velocity of $v_F = 5.5\,\mathrm{cm\,s^{-1}}$, for cakes formed on (a) the SMF medium and (b) the SG medium. The corresponding flow regimes are also indicated. The Knudsen numbers were calculated using the pore diameters described in Table 2. It can be observed that the continuum regime is not reached for either filter cakes on both filter media. Furthermore, the slip regime is only marginally attained. Consequently, when calculating the filter cake pressure drop, rarefaction effects due to the high Knudsen numbers, as well as slip effects, must be taken into account.

For the SMF medium, the filter cake pressure drops are very similar across the three repetitions, with a maximum deviation between the measurements of only about 14%. Together with the nearly constant filter cake thickness specific filter cake pressure drop, $\Delta p_{FC}/L_{FC}$, this indicates highly reproducible filter cake formation.

In contrast, for the SG medium, the curves are slightly shifted to each other. As discussed above, this can be attributed both to the use of different SG samples and to the inhomogeneous SG surface and consequently, to differences in the dust cake–specific parameters. Therefore, this leads to a much larger spread in cake masses and corresponding filter cake pressure drops, with a maximum deviation of about 78% at $p_{abs} = 5$ hPa between the measurement repetitions. Moreover, the gradient of the filter cake pressure drop curve for the SG medium is, on average, steeper than that of the SMF medium.

3.2 | Filter Cake Pressure Drop Approximation for the SMF Medium

Because the SMF data exhibit high reproducibility and narrow filter cake property scatter, the filter cakes on this filter medium

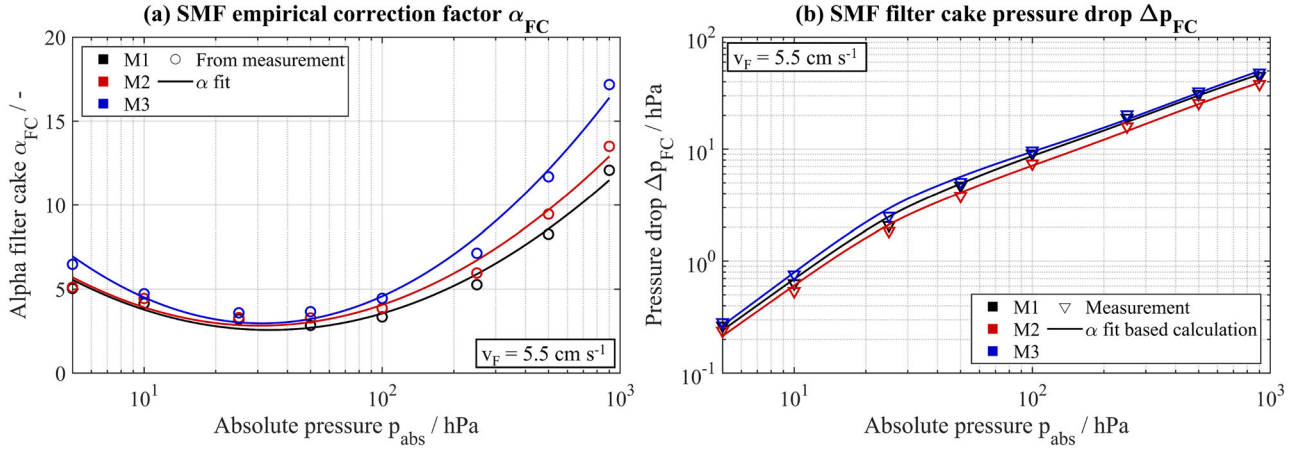

FIGURE 7 | (a) Empirical correction factor α_{FC} as a function of absolute pressure for the three different measurements for the SMF medium. Symbols represent the values of α_{FC} calculated from the measured pressure drops, while the solid line shows the fitted curve. (b) Filter cake pressure drop as a function of absolute pressure for the three repetitions at $v_F = 5.5\,\mathrm{cm\,s^{-1}}$ for the SMF medium. Symbols represent the experimental measurements and solid lines the corresponding model calculations based on the fit functions for α_{FC}.

were used first to verify the applicability of the calculation model introduced in Section 2.5.

With the cake-specific parameters given in Table 2, together with additional material and fluid-specific parameters, it is possible to determine an empirical correction factor α_{FC}. The values of α_{FC} calculated from the determined filter cake pressure drops are shown as circles in Figure 7a. The results show that α_{FC} decreases until approximately 50 hPa and then increases again. This non-monotonic behavior differs from that observed for unloaded filter media, where a linear relationship between absolute pressure and empirical correction factor α_{FM} was consistently found. Therefore, to describe the course of α_{FC} in detail, all recorded pressure drop measurements must be considered.

The course of α_{FC} can be described by the following quadratic logarithmic function:

$$\alpha_{FC} = A\,\log_{10}(p_{abs})^2 + B\,\log_{10}(p_{abs}) + C. \tag{9}$$

The fitted course of α_{FC} for the SMF medium is shown in Figure 7a as a solid line. Using this fit function, the variation of α_{FC} as a function of absolute pressure can be quantified with a coefficient of determination of $R^2 > 0.98$.

The observed nonlinear trend in α_{FC} can be explained as follows: In the work of Karniadakis et al. [23], the focus was on flow through individual long pipes with a constant cross-section. In the present study, however, the model is applied to describe complex, structured filter cakes. Consequently, the parameter α acts as a combined correction factor, accounting for both structural effects and rarefaction, rather than representing a pure rarefaction coefficient as in Karniadakis et al. In addition, flow through a filter cake is accompanied by continuous inlet and outlet effects due to its porous structure. These effects are neglected in the model of Karniadakis et al., which is based on the assumption of very long and pressure depended pipes. In this context, α_{FC} serves merely as a fitting parameter without a direct physical dependence on rarefaction effects alone.

Based on the α_{FC} profiles in Figure 7a, Equation (6) was used to back-calculate the filter cake pressure drop as a function of absolute pressure. The resulting curves are shown in Figure 7b. The largest deviation between measured and calculated filter cake pressure drop Δp_{FC} occurs at $p_{abs} = 25$ hPa for measurement 1 and amounts to 19.1%. Across the remaining operating range, deviations remain comparatively small. Overall, the calculated Δp_{FC} curves agree very well with the experimental values.

A closer look at Table 2 shows that the filter cakes on the SMF medium exhibit very similar pore diameters and porosities across the three repetitions. This motivates a reduction of experimental effort by parameter averaging. In other words, instead of characterizing each filter cake separately, it may be sufficient to determine representative mean values of the filter cake porosity $\varepsilon_{FC,mean}$ and the mean pore diameter $d_{pore,FC,mean}$ of the filter cake once and apply them for subsequent calculations.

Operationally, the workflow is as follows: First, compute representative averages of the cake porosity and mean pore diameter across the three SMF repetitions, $\bar{\varepsilon}_{FC}$ and $\overline{d}_{p,FC}$ (from Table 2). Second, using $\bar{\varepsilon}_{FC}$ and $\overline{d}_{p,FC}$, determine for each measurement an $\alpha_{FC}(p_{abs})$ profile. These three profiles are then averaged pointwise in p_{abs} to obtain a single mean $\overline{\alpha}_{FC}(p_{abs})$. Finally, $\overline{\alpha}_{FC}(p_{abs})$ is inserted into Equation (6) to back-calculate Δp_{FC}.

Figure 8a shows a scatter plot of the α_{FC} values derived from the pressure drop measurements for the SMF medium together with two fitted datasets:

- **Fit A**: uses filter-cake-specific $\varepsilon_{FC,mean}$ and $d_{pore,FC,mean}$ to compute and fit $\alpha_{FC}(p_{abs})$ for each repetition, which is then inserted into Equation (6) for back-calculating Δp_{FC}.
- **Fit B**: uses across repetition averages $\bar{\varepsilon}_{FC}$ and $\overline{d}_{p,FC}$ to form repetition specific $\alpha_{FC}(p_{abs})$ curves that are averaged into a single mean alpha profile $\overline{\alpha}_{FC}(p_{abs})$ and used in Equation (6) to compute Δp_{FC}.

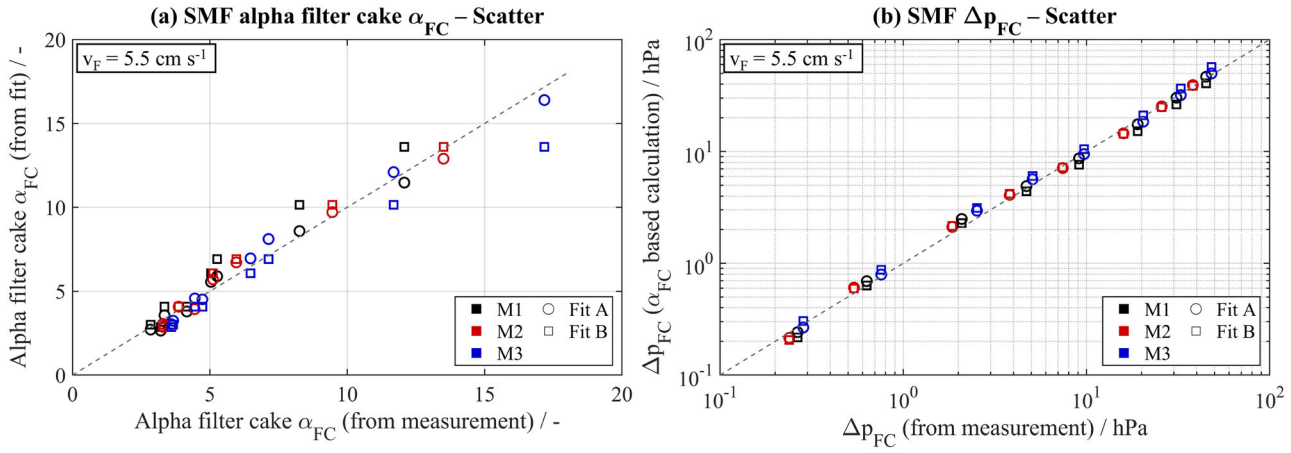

FIGURE 8 | (a) Scatter plot of the empirical correction factor α_{FC} for the three measurements and the two fits (A and B) for the SMF medium. (b) Scatter plot of the filter cake pressure drop for the three repetitions at $v_F = 5.5\,\mathrm{cm\,s^{-1}}$, showing calculated pressure drop versus measured values for the two fits for the SMF medium.

A slight scatter of the calculated α_{FC} values is observed. As expected, the Fit B points (shown as squares) are identical across repetitions at a given absolute pressure, since the same averaged parameters and mean alpha profile are used. Even when using the SMF medium specific mean $\bar{\alpha}_{FC}$, the fits remain strong, with coefficients of determination $R^2 > 0.90$ for all three repetitions, indicating very good agreement.

Figure 8b compares back-calculated and experimentally derived Δp_{FC} for both fits of the SMF medium. The largest filter-cake pressure drops occur at $p_{abs} = 900\,\mathrm{hPa}$. Along the overall trend (approximately along the 1:1 bisector), both Δp and p_{abs} decrease, reaching the smallest values at $p_{abs} = 5\,\mathrm{hPa}$. The maximum deviation for Fit B is 23.43% at $p_{abs} = 250\,\mathrm{hPa}$, for Measurement 3. In general, Fit A yields slightly smaller deviations than Fit B, as expected given its greater level of filter-cake-specific detail. Nevertheless, Fit B still produces very satisfactory agreement despite the strong simplification to a mean α_{FC}.

For a filter medium with a homogeneous surface (as for the SMF used here), it is sufficient to characterize only a limited number of filter cakes once to determine representative mean values of $\varepsilon_{FC,mean}$ and $d_{pore,FC,mean}$. These values can then be applied in subsequent investigations with only a minor loss of accuracy in Δp_{FC}. Moreover, as long as the filter cake pressure drop exhibits only limited scatter, a single mean alpha profile $\overline{\alpha}_{FC}(p_{abs})$ can be used to calculate the filter cake pressure drop with good accuracy.

The conclusions were obtained for the specific test dust used here. Applicability to other particulate systems (i.e., other particle size distributions) must be verified. The filter cake thickness and mass remain required inputs for computing Δp_{FC}. If an approximately linear relation between filter cake mass and Δp_{FC} is established in an initial calibration, L_{FC} may be estimated thereafter, avoiding repeated LSM imaging. Any such shortcut must define its validity range and be checked periodically, as nonlinear effects (e.g., compressibility, restructuring, medium imprinting) can arise and compromise accuracy.

3.3 | Filter-Cake Pressure-Drop Approximation for the SG Medium

Having established the validity of the simplified approach for the SMF medium, we next examine its applicability to the heterogeneous SG medium. Compared with the SMF medium, Table 2 shows a markedly larger scatter in the mean porosities and mean pore diameters of dust cakes formed on the SG medium and no clear linear relationship between filter cake mass, filter cake thickness, and filter cake pressure drop can be observed.

This behavior is consistent with the structure of the SG medium: a fine coating applied onto a coarse support structure leads to a strongly inhomogeneous surface. As shown by the broad pore size distribution in Appendix A, the coated SG medium still contains a noticeable fraction of comparatively large pores, which implies locally more permeable surface regions. During the initial stage of dust deposition, these regions are expected to be loaded preferentially. For the very thin filter cakes investigated here, the resulting inhomogeneities in the near-filter-medium region can still affect the cake properties and thus contribute to the larger scatter observed for the SG medium. For sufficiently thick filter cakes, in contrast, the relative influence of the substrate is expected to decrease markedly.

The empirical correction factor α_{FC} determined with measurement-specific parameters ($\varepsilon_{FC,mean}$, $d_{pore,FC,mean}$) follows the same qualitative trend as for the SMF medium (see Figure E.1): it first decreases with absolute pressure, reaches a minimum, and then increases again. The fits show good agreement, with coefficients of determination $R^2 > 0.98$ across all repetitions. However, the SG medium curves exhibit substantially greater inter-repetition scatter than observed for the SMF medium. Despite this, the back-calculated Δp_{FC} values still show good agreement with the measurements in parts of the operating range.

Against this background, the central question is whether the simplified "mean-$\overline{\alpha}_{FC}$" approach that worked for the SMF medium remains adequate for the heterogeneous SG medium. Figure 9a

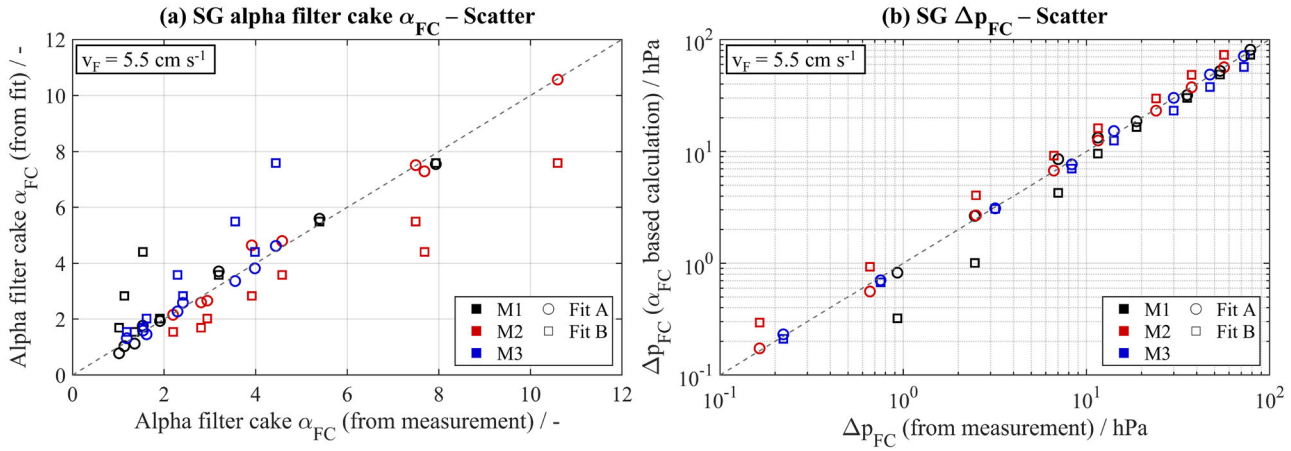

FIGURE 9 | (a) Scatter plot of the empirical correction factor α_{FC} for the three measurements and the two fits (A and B) for the SG medium. (b) Scatter plot of the filter-cake pressure drop for the three repetitions at $v_F = 5.5\,\mathrm{cm\,s^{-1}}$, showing calculated pressure drop versus measured values for the two fits for the SG medium.

displays the scatter of α_{FC} for Fits A and B (constructed analogously to the SMF case). A considerably larger spread is observed for both fits, with Fit B exhibiting clearly higher scatter than Fit A. This is reflected in the coefficients of determination, which drop to $R^2 = 0.72$ for M1, $R^2 = 0.54$ for M2, and $R^2 = 0.53$ for M3. Figure 9b compares back-calculated and experimentally derived filter cake pressure drops Δp_{FC}: for Fit A, the maximum deviation between the measured and calculated filter cake pressure drop values is 17.5% at $p_{abs} = 10\,\mathrm{hPa}$ for Measurement 2, whereas all other points remain below 12.7% deviation. For Fit B, deviations are substantially larger; the maximum occurs at $p_{abs} = 5\,\mathrm{hPa}$ for Measurement 1 with 189.4%, although reasonable agreement is obtained at some operating points. On average, the deviation for Fit B is approximately 34.7%.

These results indicate that, for very thin filter cakes formed on structurally inhomogeneous filter media (as for the SG medium studied here), the simplification using a single mean $\overline{\alpha}_{FC}$ is not well suited to predict Δp_{FC} across the full range. Instead, filter-cake-specific parameters and accordingly filter-cake-specific α_{FC} profiles should be used for the back-calculation of the filter cake pressure drop on the SG medium.

Overall, for filter cakes formed on homogeneous filter media, the experimental effort can be reduced: a small set of filter cakes may be characterized once with respect to mean porosity and mean pore diameter to derive a filter medium specific mean $\overline{\alpha}_{FC}$ for subsequent calculations. If, however, the filter medium promotes local inhomogeneities in the developing cake structure in the near-filter-medium region (as with the SG medium here, where a fine coating is applied to a coarse support structure), each filter cake must be analyzed individually and the corresponding filter-cake-specific parameters used when determining Δp_{FC}. In future investigations, this effect should be minimized by generating sufficiently thick filter cakes, especially on structurally inhomogeneous filter media, so that the substrate influence becomes less relevant for the overall cake structure.

4 | Conclusion and Outlook

This work systematically examined filter cake pressure drop under reduced absolute pressure, from near-atmospheric conditions down to 5 hPa.

Two filter media were investigated at a constant face velocity of $5.5\,\mathrm{cm\,s^{-1}}$. The first was a surface medium with a coarse sintered granular support structure and a sintered granular coating. The second was a non-woven sintered metal fiber medium. Filter cakes were formed at $p_{abs} = 900\,\mathrm{hPa}$ and the absolute pressure was then reduced stepwise. The resulting filter cake pressure drop decreased with decreasing absolute pressure.

A calculation model from Karniadakis et al., previously adapted for clean surface media, was evaluated for filter cakes by representing the cake as parallel channels and introducing an empirical correction factor α_{FC} to capture filter cake morphology and rarefaction effects. For both media, α_{FC} follows a quadratic dependence on $\ln p_{abs}$, implying that reliable identification of $\alpha_{FC}(p_{abs})$ requires measurements at multiple reduced absolute pressure levels.

On the SMF medium, filter cakes were highly homogeneous, as indicated by the small inter repetition variation of the thickness-specific pressure drop $\Delta p_{FC}/L_{FC}$. Replacing filter-cake-specific porosity and pore diameter by representative averages and using the corresponding mean $\overline{\alpha}_{FC}(p_{abs})$ yielded back-calculated Δp_{FC} values in very good agreement with the measurements (maximum deviations on the order of a few tens of percent, typically much smaller), confirming that parameter averaging together with a mean α_{FC} is adequate for homogeneous filter cakes.

By contrast, for the SG medium, the substantially larger scatter in filter cake properties indicates that the structure of the filter medium can still influence the developing cake structure in the near-filter-medium region. This effect is particularly relevant here because the investigated filter cakes are very thin.

Accordingly, the observed variability should not be interpreted as evidence that the entire filter cake is strongly inhomogeneous. Rather, it shows that locally inhomogeneous cake formation at the beginning of deposition can still affect the measured cake behavior when the cakes are thin. Under these conditions, a single mean $\overline{\alpha}_{FC}$ is insufficient, and filter-cake-specific parameters together with filter-cake-specific $\alpha_{FC}(p_{abs})$ profiles must be retained for accurate back calculation of the filter cake pressure drop.

Future work should test additional dusts to isolate how particle size distribution and shape affect α_{FC} and filter cake permeability. In addition, especially for structurally inhomogeneous filter media, the filter cake thickness above which the influence of the underlying substrate becomes negligible should be determined. Such investigations would help to identify the transition from substrate influenced cake formation to a regime with sufficiently thick and statistically homogeneous filter cakes. Furthermore, the regeneration behavior of surface filters at low absolute pressure and the separation efficiency of surface filter media as a function of absolute pressure should be investigated.

Nomenclature

Symbols

Latin Symbols

A_F	Filter face area, m^2
A_{pore}	Cross-sectional area of a pore, m^2
a	Characteristic length, m
b	Slip coefficient, –
C_{FC}	Specific filter cake constant, –
C_1	Auxiliary constant, $m\,Pa^{-1}$
C_2	Auxiliary constant, Pa
d	Molecular diameter of air, m
$d_{pore,mean}$	Mean pore diameter, m
$d_{pore,FM,mean}$	Mean filter medium pore diameter, m
$d_{pore,FC,mean}$	Mean filter cake pore diameter, m
k_B	Boltzmann constant, $J\,K^{-1}$
Kn	Knudsen number, –
L	Thickness, m
L_{FC}	Filter cake thickness, m
L_{FM}	Filter medium thickness, m
m_{FC}	Filter cake mass, kg
p_{abs}	Absolute upstream pressure, hPa
p_i	Pressure immediately upstream of the filter cake, hPa
p_o	Pressure downstream of the filter cake, hPa
Q_0	Cumulative pore size distribution, –
t	Time, s
T	Temperature, K
v_F	Filter face velocity, $m\,s^{-1}$
v_{pore}	Pore velocity, $m\,s^{-1}$
$\dot{V}$	Volumetric flow rate through a single pore, $m^3\,s^{-1}$
W_{FC}	Filter cake areal mass, $g\,m^{-2}$
W_{FM}	Filter medium basis weight, $g\,m^{-2}$
$x_{50,3}$	Volume-based median particle diameter, µm
Δp_{FC}	Pressure drop across the filter cake, hPa
Δp_{FM}	Pressure drop across the filter medium, hPa
Δp_{Tot}	Total pressure drop, hPa

Greek symbols

α_{FC}	Empirical correction factor for the filter cake, –
α_{FM}	Empirical correction factor for the filter medium, –
ε	Porosity, –
$\varepsilon_{FC,mean}$	Mean filter cake porosity, –
$\varepsilon_{FM,mean}$	Mean filter medium porosity, –
λ	Mean free path, m
μ_L	Dynamic viscosity of air, Pa s
ρ_{FC}	Filter cake density, $kg\,m^{-3}$
ρ_{FM}	Filter medium density, $kg\,m^{-3}$
ρ_L	Gas density, $kg\,m^{-3}$
ρ_P	Particle density, $kg\,m^{-3}$

Subscripts

abs	Absolute, –
FC	Filter cake, –
FM	Filter medium, –
i	Inlet / upstream, –
mean	Mean value, –
o	Outlet / downstream, –
pore	Pore, –
Tot	Total, –

Author Contributions

Vanessa Löschner: methodology, software, validation, formal analysis, investigation, data curation, writing – original draft, visualization, project administration. **Jörg Meyer**: conceptualization, formal analysis, writing – review and editing. **Achim Dittler**: conceptualization, resources, writing – review and editing, supervision, funding acquisition.

Acknowledgments

We gratefully acknowledge that this project was funded by the Deutsche Forschungsgemeinschaft (DFG, German Research Foundation) – 541566488. We acknowledge the collaboration of Herding GmbH Filtertechnik for providing the SG filter medium and Bekaert SA for providing the SMF medium used in this work. During the preparation of this manuscript, the authors used ChatGPT (OpenAI) to improve language clarity and readability. All scientific content, interpretations and conclusions were produced and verified by the authors. The authors take full responsibility for the accuracy and integrity of the work. Parts of this work were presented at WFC 2025 in Bordeaux.

Open access funding enabled and organized by Projekt DEAL.

Funding

This research was funded by the Deutsche Forschungsgemeinschaft (DFG, German Research Foundation), grant number: 541566488.

Conflicts of Interest

The authors declare no conflicts of interest.

Data Availability Statement

The data that support the findings of this study are available from the corresponding author upon reasonable request.

References

1. A. B. Jindal, *Pharmaceutical Process Engineering and Scale-Up Principles*, Vol. 13, AAPS Introductions in the Pharmaceutical Sciences (Springer Nature, 2023).

2. C. E. Orrego, N. Salgado, and L. F. Sarmiento, "Freeze Drying and Vacuum Drying," in: Drying Technology in Food Processing (2023): 203–240.

3. A. I. Amjad, "Filtration in Pharmaceutical Industries and Role of Textile," *TEKS* 65, no. 3 (2022): 227–241.

4. T. C. Smith, "Detection and Control of Particles in Vacuum Environments for Semiconductor Processing," in *Particles in Gases and Liquids 2: Detection, Characterization, and Control*, ed. K. L. Mittal (Springer, 1990), 61–74.

5. M. Bohnet and F. Ullmann, *Ullmann's Encyclopedia of Industrial Chemistry*, 6th ed. (Wiley-VCH, 2003).

6. W. Jorisch, *Vakuumtechnik: In der Chemischen Industrie* (Wiley-VCH, 1999).

7. M. W. Jornitz, *Filtration and Purification in the Biopharmaceutical Industry*, 3rd ed., Drugs and the Pharmaceutical Sciences (CRC Press, Taylor & Francis Group, 2020).

8. C. M. Van'T Land, *Drying in the Process Industry*, 1st ed. (Wiley, 2011).

9. L. Wu, *Rarefied Gas Dynamics: Kinetic Modeling and Multi-Scale Simulation* (Springer Nature, 2022).

10. D. Richter, *Mechanik der Gase*, Springer-Lehrbuch (Springer, 2010).

11. J. Pich, "der Druckabfall der Faserfilter in molekularer Strömung," *Staubreinhaltung der Luft* 29 (1969): 407–408.

12. P. Li, C. Wang, Y. Zhang, and F. Wei, "Air Filtration in the Free Molecular Regime: A Review of High-Efficiency Particulate Air Filters Based in Carbon Nanotubes," *Small* 10, no. 22 (2014): 4543–4561.

13. Z. Liu, D.-R. Chen, P. Wang, and Z. Ji, "Effect of Filtration Pressure on the Particle Penetration Efficiency of Fibrous Filter Media," *Separation and Purification Technology* 274 (2021): 119086.

14. J. A. Hubbard, J. E. Brockmann, J. Dellinger, D. A. Lucero, A. L. Sanchez, and B. L. Servantes, "Fibrous Filter Efficiency and Pressure Drop in the Viscous-Inertial Transition Flow Regime," *Aerosol Science and Technology* 46, no. 2 (2012): 138–147.

15. Z. Zhang and B. Y. H. Liu, "Experimental Study of Aerosol Filtration in the Transition Flow Regime," *Aerosol Science and Technology* 16, no. 4 (1992): 227–235.

16. M. He, S. Dhaniyala, and M. Wagner, "Characterization of Filter Performance Under Low-Pressure Operation," *Aerosol Science and Technology* 50, no. 5 (2016): 417–428.

17. J. Pich, "Pressure Drop of Fibrous Filters at Small Knudsen Numbers," *Annals of Occupational Hygiene 9* (1966): 23–27.

18. J. Pich, "Pressure Characteristics of Fibrous Aerosol Filters," *Journal of Colloid and Interface Science* 37 (1971): 912–917.

19. C. N. Davies, *Air Filtration* (Academic Press, 1973).

20. R. C. Brown, *Air Filtration: An Integrated Approach to the Theory and Applications of Fibrous Filters* (Pergamon Press, 1993).

21. M. Robinson and H. Franklin, "The Pressure Drop of a Fibrous Filter at Reduced Ambient Pressure," *Journal of Aerosol Science* 3, no. 6 (1972): 413–427.

22. Y. M. Glushkov, "Resistance of Fibrous Filters in Free Molecule Flow," *Fluid Dynamics* 3, no. 4 (1972): 119–122.

23. G. Karniadakis, A. Beşkök, and N. Aluru, *Microflows and Nanoflows: Fundamentals and Simulation*, Interdisciplinary Applied Mathematics (Springer, 2005).

24. A. Beskok and G. E. Karniadakis, "Report: A model for Flows in Channels, Pipes, and Ducts at Micro and Nano Scales," *Microscale Thermophysical Engineering* 3, no. 1 (1999): 43–77.

25. V. Löschner, J. Meyer, and A. Dittler, "Experimental and Theoretical Investigation of the Pressure Drop Acrosss Different Surface Filter Media at Low Absolute Pressures Down to 100 Pa," *Separation and Purification Technology* 361 (2025): 131093.

26. V. Löschner, J. Lüttmann, J. Meyer, and A. Dittler, "Dust Cake Build-Up on Gas Cleaning Surface Filters at Ambient and Low Absolute Pressure," *Separation and Purification Technology* 381 (2026): 135536.

27. S. S. R. Cirqueira, E. H. Tanabe, and M. L. Aguiar, "Evaluation of Operating Conditions During the Pulse Jet Cleaning Filtration Using Different Surface Treated Fibrous Filters," *Process Safety and Environmental Protection* 105 (2017): 69–78.

28. H. E. Kolb, R. Schmitt, A. Dittler, and G. Kasper, "On the Accuracy of Capillary Flow Porometry for Fibrous Filter Media," *Separation and Purification Technology* 199 (2018): 198–205.

Appendix A: Cumulative Pore Size Distribution

Figure A.1 shows the cumulative pore size distributions $Q_0(d_{\text{pore}})$ of the SG medium with and without PPS coating, determined by porometry according to the procedure described in [28]. For each medium, five different samples were analyzed. The mean distribution is shown together with the corresponding standard deviation as a shaded band, and the median pore diameter d_{50} is indicated by a dashed line.

The PPS-coated SG medium exhibits a pronounced fraction of small pores below approximately 10 µm, which is attributed to the surface coating. This is also reflected by the shift of the median pore diameter from

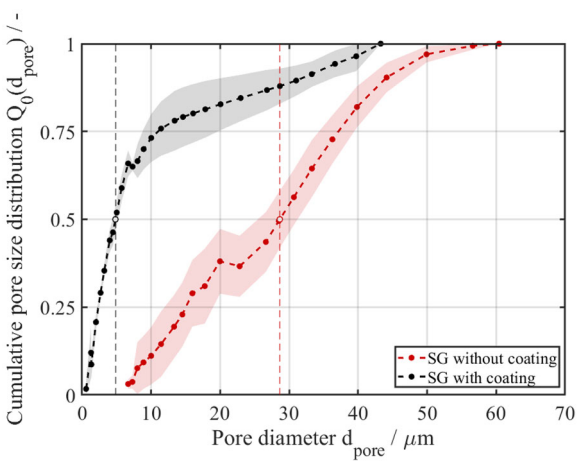

FIGURE A.1 | Cumulative pore size distribution $Q_0(d_{\text{pore}})$ of the SG medium with and without PPS coating. The dashed vertical lines indicate the median pore diameter d_{50}. The distributions were determined by porometry from five samples per medium. Shaded areas represent the standard deviation.

$d_{50} = 28.64$ µm for the uncoated medium to $d_{50} = 4.82$ µm for the coated medium. At the same time, the coated medium still exhibits a noticeable fraction of larger pores extending to more than 40 µm. This overlap with the pore size range of the uncoated medium indicates that the PPS layer is neither fully homogeneous nor fully surface-covering.

The broader pore size distribution of the coated medium is also reflected by the span, defined as $(d_{90} - d_{10})/d_{50}$. The uncoated medium yields a span of 1.46, whereas the coated medium shows a substantially larger value of 6.29. Thus, the pore size distribution provides a quantitative description of the structural inhomogeneity of the coated SG medium.

The slight kink visible in both $Q_0(d_{pore})$ curves originates from the switching between two mass flow controllers during the porometry measurement. The transition between the two controllers, which are used for different flow ranges, leads to a small discontinuity in the recorded signal. Because this effect occurs in both media, it is attributed to the measurement procedure and not to a structural property of the investigated pore system.

Appendix B: Validation of the Clean Filter Medium Pressure Drop Scaling Approach

As described in Section 2.4, the filter cake build-up method used in this work does not allow a direct determination of the clean filter medium pressure drop Δp_{FM} at every absolute pressure stage for each individual sample. For the SG medium, only the value at 900 hPa was measured directly for each sample. The remaining values were obtained by scaling the sample-specific Δp_{FM} at 900 hPa with the pressure stage ratios of a representative reference dataset. This procedure assumes that the relative pressure dependence of Δp_{FM} is sample invariant.

To assess this assumption, additional clean filter medium measurements were carried out for both the SG and SMF media. Figure B.1 compares predicted and directly measured values of Δp_{FM}. The x-axis shows the directly measured Δp_{FM} values of sample B, while the y-axis shows the corresponding values predicted for sample B using the scaling approach described in the main text, based on the pressure dependence of a different reference Sample A. For the SG medium, this provides a direct validation of whether the scaling approach can be transferred between different samples. For the SMF medium, the same comparison was intentionally carried out with a second sample that was not used in the main experiments, in order to test the general validity of the approach beyond the originally investigated sample.

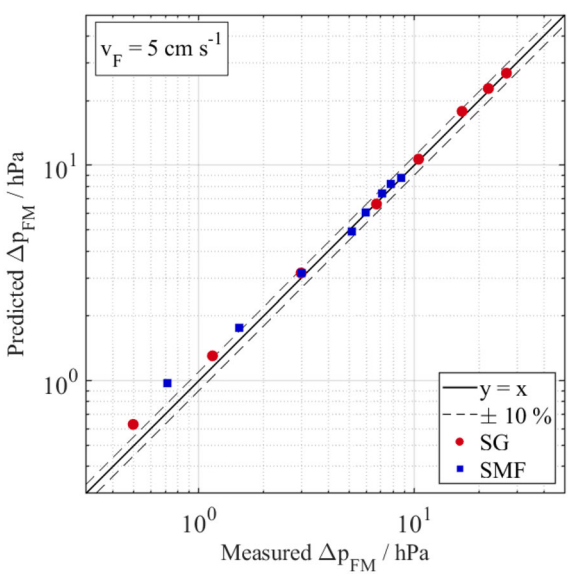

FIGURE B.1 | Comparison of predicted and measured clean filter medium pressure drops Δp_{FM} at $v_F = 5\,\mathrm{cm\,s^{-1}}$ for the SG and SMF media. The x-axis shows the directly measured values of one sample, whereas the y-axis shows the corresponding values predicted from the pressure dependence of a different reference sample using the scaling approach described in the main text. The solid line indicates $y = x$, and the dashed lines indicate a deviation of ±10 %.

The results show good agreement between prediction and measurement for both media. The data points at the upper end of the bisector correspond to the highest absolute pressure stages, whereas decreasing Δp_{FM} along the axes corresponds to decreasing absolute pressure. Except for the lowest absolute pressure stages, the deviation remains below ±10 %. At the lowest absolute pressure stages, the relative deviation increases, but the corresponding absolute Δp_{FM} values are very small. Accordingly, these larger relative differences correspond to only small absolute deviations and do not change the overall assessment. This confirms that the scaling approach provides a sufficiently accurate approximation of the clean filter medium pressure drop over the investigated pressure range. Accordingly, the assumption of an approximately sample-invariant pressure dependence of Δp_{FM} is considered justified for the present evaluation.

Appendix C: Pressure Drop Evolution During Dust Deposition and Filter Cake Build-Up

Figure C.1 illustrates the pressure drop evolution during dust deposition and the subsequent filter cake build-up at ambient pressure. Figure C.1a shows representative $\Delta p_{Tot}(t)$ curves for the SG and SMF media. In the following, the SG medium is discussed first. For the SG medium, a pronounced steep increase in $\Delta p(t)$ is observed immediately after aerosol connection. In principle, this behavior can be attributed to three possible causes, namely internal deposition within the filter medium (depth filtration), compensation of surface inhomogeneities by preferential deposition in highly permeable regions, and elevated particle concentrations during the start-up of the raw gas generation. If internal deposition were the dominant mechanism, one would expect an initially rather slow increase that gradually turns into a progressive rise before the linear cake build-up regime is reached. In contrast, compensation of surface inhomogeneities would rather lead to an initially very steep increase followed by a degressive course that gradually approaches the later linear cake build-up regime. Concentration fluctuations mainly affect the slope of the $\Delta p(t)$ curve and would therefore result in a steeper increase at higher concentration and a flatter increase at lower concentration. Based on the measured $\Delta p_{Tot}(t)$ course, the pronounced steep increase in $\Delta p(t)$ for the SG medium therefore suggests that compensation of surface inhomogeneities and the elevated particle concentration at the beginning of the experiment are the dominant contributions. Internal deposition within the filter medium cannot be excluded completely, but it cannot be identified unambiguously from the pressure drop curves alone. This interpretation is consistent with the broad pore size distribution of the SG medium discussed in Appendix A, which indicates the presence of preferentially permeable surface regions. After the steep increase in $\Delta p(t)$, an approximately linear cake build-up phase is observed. At the end of the experiment, the aerosol is disconnected, which causes an additional system-related pressure change before the final total pressure drop is recorded.

The corresponding $\Delta p_{Tot}(t)$ curve of the SMF medium is also shown in Figure C.1a. Here, the steep increase in $\Delta p(t)$ at the beginning is clearly less pronounced than for the SG medium. Since the SMF surface is considerably more homogeneous, this smaller initial effect is likely caused mainly by the elevated particle concentration during aerosol start-up. However, this interpretation cannot be proven directly from the present data.

In Figure C.1a, the dotted line represents a simplified description in which the full pressure drop increase during dust deposition is assigned to the subsequent cake evaluation. A more detailed physical description is given

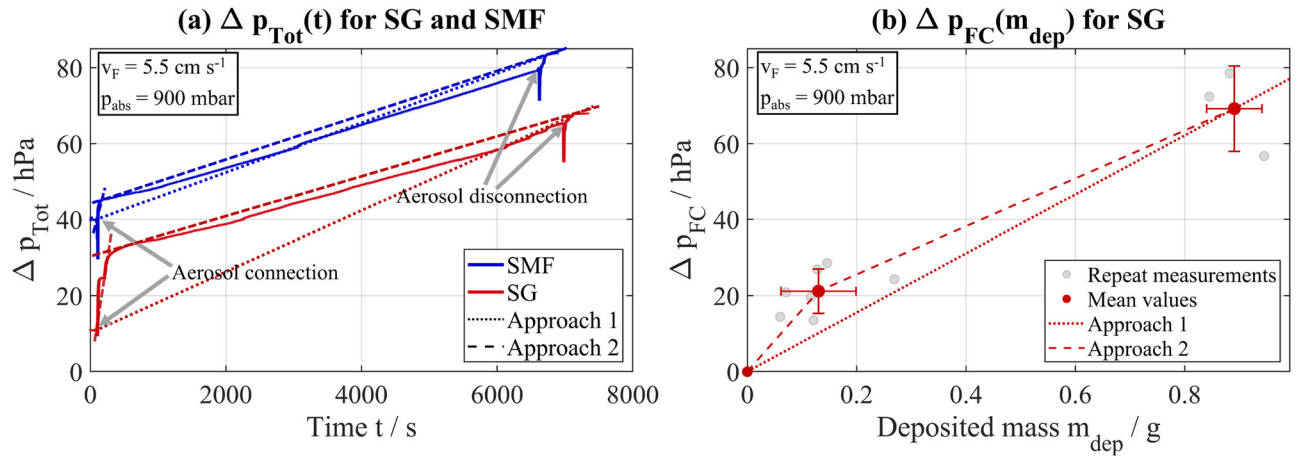

FIGURE C.1 | Pressure drop evolution during dust deposition and filter cake build-up at ambient pressure. (a) Representative total pressure drop curves $\Delta p_{\mathrm{Tot}}(t)$ for the SG and SMF media. The dotted lines indicate a simplified description in which the full pressure drop increase during dust deposition is considered (Approach 1). The dashed lines indicate a more refined description in which the initial transition region is excluded and only the subsequent quasi-linear increase is attributed to filter cake build-up (Approach 2). (b) Pressure drop increase of the SG medium as a function of deposited mass. Gray symbols show individual values and red symbols show mean values. The lower data cluster corresponds to additional characterization experiments focusing on the initial transition region, while the upper data cluster represents the regular cake build-up experiments. The dotted line represents Approach 1, while the dashed line represents Approach 2.

by the dashed line, in which the initial transition region is excluded and only the subsequent quasi-linear increase is attributed to filter cake build-up. In the following, these two descriptions are referred to as Approaches 1 and 2, respectively.

A representation of $\Delta p(t)$ solely as a function of time is not sufficient to assess the transition between the initial deposition phase and the subsequent cake build-up, because it does not account for concentration fluctuations during the experiment. Therefore, Figure C.1b shows the corresponding Δp increase as a function of deposited mass for the SG medium. In such a representation, the regular cake build-up experiments of the main study provide only two characteristic points, namely the origin and the final deposited mass with its corresponding Δp increase, since no online measurement of the deposited mass was available. This two-point representation corresponds to Approach 1. However, because a substantial deposited mass is already present after the steep increase in $\Delta p(t)$, an additional point is required to characterize the end of the initial transition region and to describe the cake build-up more meaningfully. For this reason, additional characterization experiments were performed. The resulting three-point representation corresponds to Approach 2 and allows a more refined description of the transition between initial deposition and the subsequent quasi-linear cake build-up.

Accordingly, only three characteristic mass coordinates can be assigned in Figure C.1b, namely the origin (0, 0), an intermediate point characterizing the end of the initial transition region, and the final values of the three regular cake build-up experiments reported in the main manuscript. When transferred from the time axis to the mass axis, the initially very steep increase in $\Delta p_{\mathrm{Tot}}(t)$ becomes noticeably flatter. This already indicates that the deviation introduced by Approach 1 is less severe than the $\Delta p_{\mathrm{Tot}}(t)$ representation alone might suggest.

To determine the intermediate point, seven additional characterization experiments were conducted with the SG medium, focusing only on the beginning of dust deposition. For these experiments, the pressure drop increase and the deposited dust mass at the end of the steep increase in $\Delta p(t)$ were determined. In addition, LSM images were recorded to visualize the dust distribution on the filter surface. On average, the end of the initial transition region was reached at a deposited mass of approximately $m^* \approx 0.13\,\mathrm{g}$ and a pressure drop increase of approximately $\Delta p^* \approx 21\,\mathrm{hPa}$. This deposited mass already corresponds to about 15 % of the mean final deposited mass of the regular cake build-up experiments ($m_{\mathrm{end}} \approx 0.89\,\mathrm{g}$). The lower data cluster in Figure C.1b therefore represents the additional characterization experiments focusing on the initial transition region, while the upper data cluster corresponds to the regular cake build-up experiments. The LSM images showed that a large part of the filter surface was already covered with dust, while smaller uncovered regions still remained. This supports the assumption that, during the initial loading phase of the SG medium, the easily permeable regions are loaded first.

For the specific parameter set of the additional SG experiments at ambient pressure, a transition point between the steep increase in $\Delta p(t)$ and the subsequent quasi-linear region can therefore be approximated. In this case, Approach 2 could be applied. However, corresponding characterization data are not available for the other parameter sets of the manuscript, and in particular not for reduced absolute pressures. Thus, the deposited mass present at the end of the initial transition region is unknown for these conditions. Applying Approach 2 throughout the entire study would therefore require additional assumptions that are currently not experimentally validated. For this reason, the present work accepts the approximation associated with Approach 1 rather than combining different calculation methods for different parameter sets. The resulting uncertainty is instead estimated from the difference between both approaches.

A simple estimate of this effect can be obtained by comparing the mass-specific pressure drop increase of both limiting descriptions. For Approach 1, in which the full loading interval is attributed to cake build-up, the corresponding slope is

$$k_{\mathrm{all}} = \frac{\Delta p_{\mathrm{end}}}{m_{\mathrm{end}}}.$$

For Approach 2, in which only the quasi-linear region after the initial transition is attributed to cake build-up, the corresponding slope is

$$k_{\mathrm{lin}} = \frac{\Delta p_{\mathrm{end}} - \Delta p^*}{m_{\mathrm{end}} - m^*}.$$

The relative deviation introduced by using the full loading interval can then be estimated by

$$\varepsilon_k = \frac{k_{\mathrm{all}} - k_{\mathrm{lin}}}{k_{\mathrm{lin}}}.$$

Using the mean values shown in Figure C.1b, this estimate is on the order of 20 %. Since the additional characterization experiments were only conducted for the SG medium, this value should be understood as a conservative worst case estimate for the uncertainty introduced by the evaluation approach. For the SMF medium, no corresponding characterization experiments were carried out. However, the steep increase in $\Delta p(t)$ is visibly less pronounced than for the SG medium, indicating that the associated uncertainty is expected to be smaller. In addition, the estimate should be regarded as conservative because part of the deposited dust in the initial transition region already contributes to surface coverage and early cake build-up. Accordingly, this value is not used as a direct correction of the model, but rather as an estimate of the uncertainty associated with assigning the full pressure drop increase to filter cake formation.

Appendix D: Mean Pore Diameter Variation in the Calculation Model for an Exemplary Dataset

The calculation model in Section 2.5 requires several parameters (L_{FC} (filter cake thickness), m_{FC} (filter cake mass), ε_{FC} (mean filter cake porosity), and the filter cake pressure drop Δp_{FC}). Only some of them can be directly obtained from measurements. The mean dust cake pore diameter must be inferred from a constitutive relation. Here, we employ the Carman–Kozeny equation (Equation 8) to estimate the filter cake pore diameter $d_{pore,FC}$. This constitutes a strong simplification for determining $d_{pore,FC}$, but Carman–Kozeny was chosen because the resulting $d_{pore,FC}$ values yield predictions that are well suited for the model calculations. Notably, the model can be highly sensitive to variations in pore diameter.

To illustrate this sensitivity, Figure D.1a shows the empirical correction factor α_{FC} computed for a variation of $d_{pore,FC}$ from 0.05 to 4 µm (with 0.5 µm being the Carman–Kozeny value, labeled in red). The calculations assume a constant filter face velocity, a constant porosity of $\varepsilon_{FC} = 0.84$, a dust cake mass $m_{FC} = 1.38$ g, a dust cake thickness $L_{FC} = 211$ µm and the measured total pressure drop data of the SMF medium for Measurement 3; all auxiliary parameters are taken from the same experiment (SMF Medium M3). This analysis is intended as an example to demonstrate the effect of varying $d_{pore,FC}$ on α_{FC}. As $d_{pore,FC}$ decreases, the α_{FC} curves shift upward. For increasing $d_{pore,FC}$, α_{FC} remains similar at low absolute pressure but decreases progressively at higher p_{abs}, eventually becoming negative.

Figure D.1b presents the corresponding back-calculated filter cake pressure drops derived from the fitted α_{FC} functions, alongside the experimental data. Table D.1 lists, for each $d_{pore,FC}$, the maximum deviation between model and experiment and the absolute pressure at which this deviation occurs. The Carman–Kozeny diameter $d_{pore} = 0.5$ µm yields the smallest maximum deviation with only 10.4% at $p_{abs} = 50$ hPa. Decreasing $d_{pore,FC}$ has only a modest effect on accuracy, whereas increasing $d_{pore,FC}$ leads to rapidly growing deviations; for $d_{pore} = 2.2$ µm a solution cannot be found at absolute pressures near to 250 hPa. For completeness, $d_{pore} = 4$ µm is also shown, for which the non-solvable ranges become even more pronounced. This behavior primarily arises because, beyond a certain negative α_{FC} threshold, the calculation model no longer admits a numerical solution.

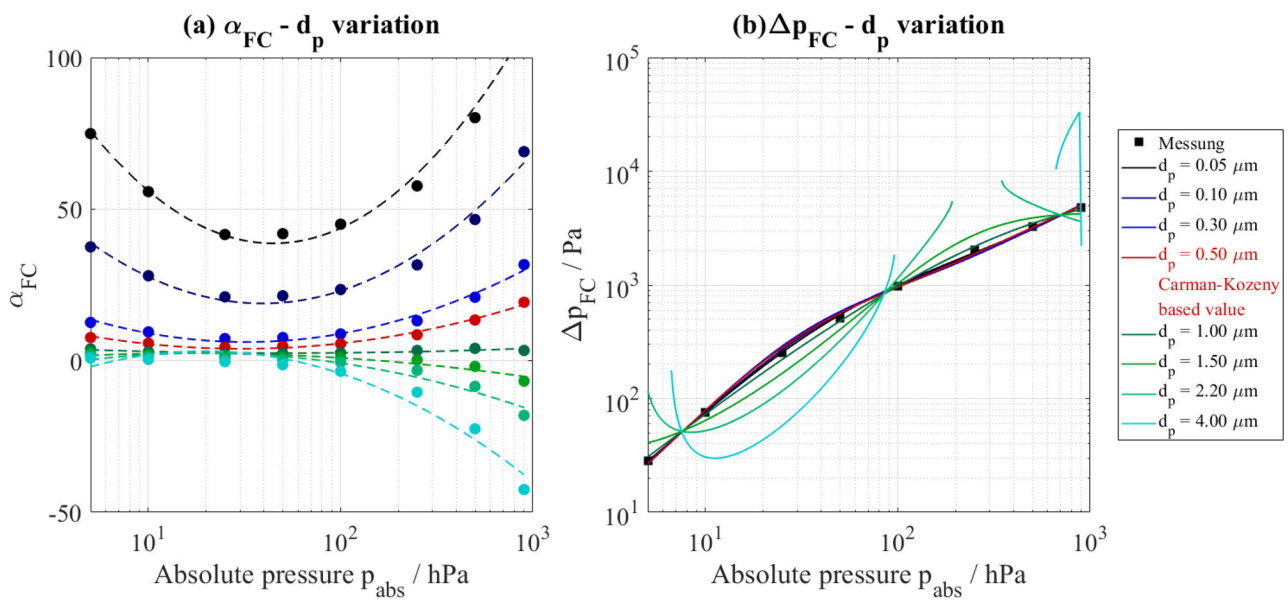

FIGURE D.1 | (a) Empirical correction factor α_{FC} as a function of absolute pressure for variations of the mean pore diameter $d_{pore,FC}$. Symbols show α_{FC} values calculated from measured pressure drops for the SMF medium (Measurement 3 [M3]); the dashed line shows the fitted curve. (b) Filter-cake pressure drop as a function of absolute pressure for the $d_{pore,FC}$ variations at $v_F = 5.5\,\mathrm{cm\,s^{-1}}$. Symbols denote experimental data; solid lines are model determinations based on the fitted α_{FC} functions.

TABLE D.1 | Maximum deviation (in %) between calculated and measured Δp_{FC} for the $d_{pore,FC}$ variations, together with the absolute pressure p_{abs} at which the maximum deviation occurs.

Mean pore diameter $d_{pore,FC}$ / µm	**0.05**	**0.10**	**0.30**	**0.50**	**1**	**1.5**	**2.2**	**4**
Maximum deviation / %	10.8	10.9	14.6	10.4	12.711	43.384	309.13	46535
Absolute pressure at max. deviation / hPa	50	50	50	25	25	5	5	5

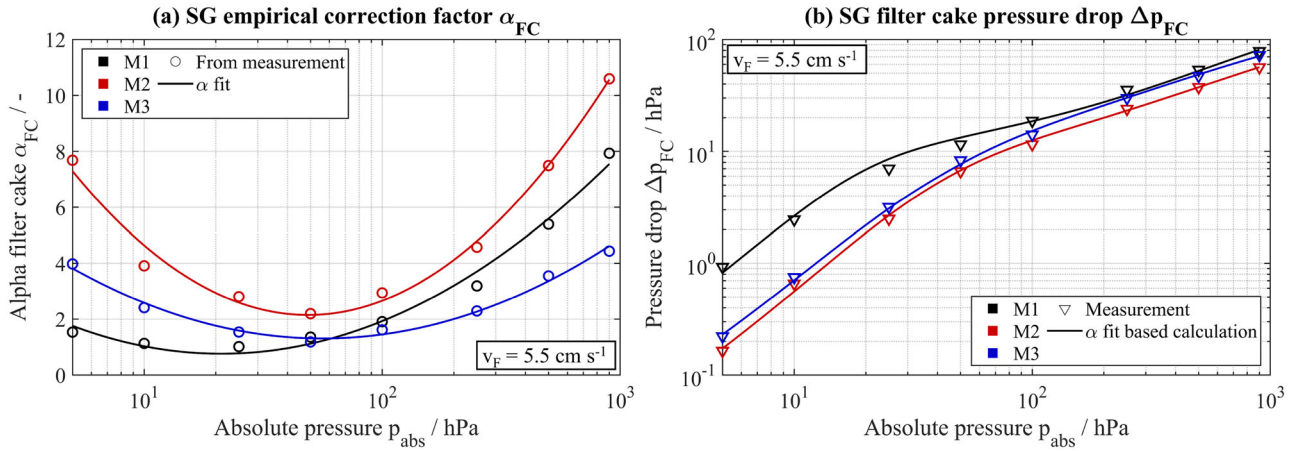

FIGURE E.1 | (a) Empirical correction factor α_{FC} as a function of absolute pressure for the three different measurements for the SG medium. Symbols represent the values of α_{FC} calculated from the measured pressure drops, while the solid line shows the fitted curve. (b) Filter cake pressure drop as a function of absolute pressure for the three repetitions at $v_F = 5.5\,\mathrm{cm\,s^{-1}}$ for the SG medium. Symbols represent the experimental measurements and solid lines the corresponding model calculations based on the fit functions for α_{FC}.

Appendix E: Filter Cake Pressure Drop Determination for the SG Medium With Filter-Cake-Specific Parameters

Figure E.1 illustrates the empirical correction factor α_{FC} and the corresponding filter cake pressure drop calculations for the SG medium using filter-cake-specific parameters. The α_{FC} profiles in Figure E.1a show a characteristic decrease with decreasing absolute pressure, followed by a minimum and a subsequent increase at low pressures, similar to the SMF medium. Notably, the quadratic logarithmic fit employed for $\alpha_{FC}(p_{abs})$ provides an excellent description for all three repetitions on SG as well, capturing the overall trend despite the larger scatter. The resulting back-calculated pressure drops in Figure E.1b agree satisfactorily with the experimental data, confirming that the model reproduces the measured Δp_{FC} when filter-cake-specific parameters and the quadratic–log fit for α_{FC} are used.